LETTER

Effect of the Charge Balance on High-Efficiency Blue-Phosphorescent Organic Light-Emitting Diodes

Neetu Chopra, Jaewon Lee, Ying Zheng, Sang-Hyun Eom, Jiangeng Xue, and Franky So*

Department of Materials Science and Engineering, University of Florida, Gainesville, Florida 32611

ABSTRACT The charge balance in blue-phosphorescent devices was studied using single-carrier devices, and the results show that the transport is highly hole dominant. The effect of the charge balance on the device performance was further demonstrated using different electron-transport materials with different electron mobilities. By optimization of the charge balance, a maximum current efficiency of 60 Cd A^{-1} at a luminance of 500 cd m^{-2} was achieved.

KEYWORDS: OLEDs • blue phosphorescence • charge balance • single-carrier devices

Organic light emitting diodes (OLEDs) have recently received a lot of attention because of their potential applications in solid-state lighting and flat-panel displays (1, 2). For white light and full-color displays, high-efficiency red, green, and blue OLEDs are required. Compared to fluorescent OLEDs, the performance of phosphorescent OLEDs is significantly better because both singlet and triplet excitons can be harvested for light emission (3). Moreover, high-efficiency OLEDs require good control of the charge balance (4). An imbalance in charge transport leads to the accumulation of charges in an OLED heterostructure, thereby resulting in a loss of efficiency (5) and lifetime (6).

However, carrier transport in most OLED devices is highly imbalanced (7). For example, the hole mobility in commonly used organic hole-transport materials such as 4,4′-bis[*N*-(1-naphthyl)-*N*-phenylamino]biphenyl (NPD) or 1,1-bis[(di-4-tolylamino)phenyl]cyclohexane (TAPC) (8, 9) is about 3 orders of magnitude higher than the electron mobility of electron-transport materials (ETMs) such as tris(8-quinolinolato)aluminum (Alq_3) or 2,9-dimethyl-4,7-diphenyl-1,10-phenanthroline (BCP) (10). In addition, triplet energies of commonly used hole-transport materials and ETMs such as NPD (triplet energy, T_1 = 2.29 eV) (11), BCP (T_1 = 2.5 eV) (12), and Alq_3 (T_1= 2.0 eV) (12) are lower than that of the commonly used blue-phosphorescent dopant iridium(III) bis[(4,6-difluorophenyl)pyridinato-*N*,*C*2′]picolinate (FIrpic, T_1 = 2.7 eV) (13), and charge imbalance leads to triplet exciton quenching. Therefore, charge balance plays an important role in achieving high-efficiency phosphorescent OLEDs. In this letter, we investigate the charge balance in FIrpic-based OLEDs by studying the charge-transport properties of the corresponding electron- and hole-only devices. The device data indicate that the carrier transport is strongly hole dominant and the recombination zone is located at the electron-transport layer (ETL) interface. Using a high-mobility, high-triplet-energy ETM, we were able to enhance the charge balance, and a maximum current efficiency of 60 cd A^{-1} at a luminance of 500 cd m^{-2} was achieved.

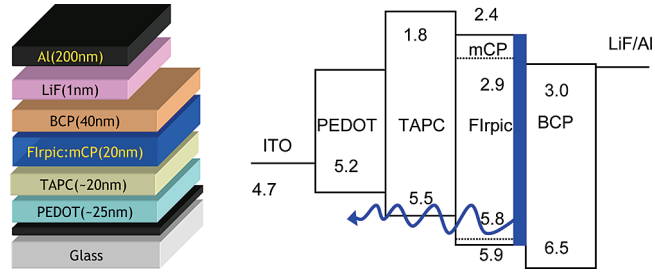

FIGURE 1. (a) Device structure and (b) energy-level diagram of the blue-phosphorescent OLED used in this study showing the location of the recombination zone.

Parts a and b of Figure 1 show the device structure of the OLED and its corresponding energy band diagram. The device has the following structure: poly(3,4-ethylenedioxythiophene)/poly(styrenesulfonic acid) (PEDOT:PSS; Clevios AI 4083, 25 nm) as the hole injection layer, TAPC (20 nm) as the hole-transport layer (HTL), 3,5′-*N*,*N*′-dicarbazolebenzene (mCP; 20 nm) doped with 2−3% FIrpic as the emitting layer (EML), BCP (40 nm) as the hole blocker, and ETL/LiF (1 nm) and Al (100 nm) as the cathode. LiF and Al were purchased from Aldrich, and all small-molecule materials used for OLED fabrication were purchased from Luminescence Technology Corp. All materials were used as received.

Prepatterned indium−tin oxide (ITO) substrates with a sheet resistance of 20 Ω per square were used for device fabrication. Substrates were first cleaned via sonication in detergent, deionized water, acetone, and isopropyl alcohol followed by UV/ozone treatment. To fabricate the OLED devices, a PEDOT:PSS layer was first spin-coated on the ITO glass substrates, and the film was then baked at 180 °C. All other layers were vacuum deposited at a pressure of 2 × 10^{-6} Torr. Luminance−current−voltage (LIV) characteristics of the OLEDs were measured using a Keithley 2400 source

* To whom correspondence should be addressed. E-mail: fso@mse.ufl.edu.
Received for review April 3, 2009 and accepted May 18, 2009

DOI: 10.1021/am900228b

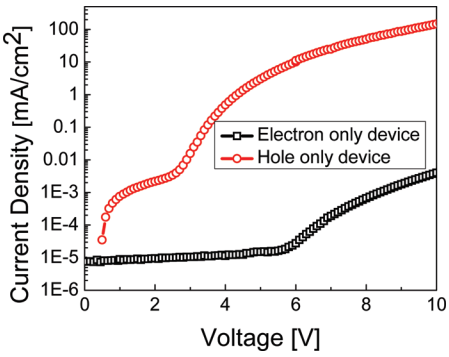

FIGURE 2. $J-V$ characteristics for hole- and electron-only devices.

meter coupled with a Keithley 6485 picoammeter along with a calibrated silicon photodiode for photocurrent measurements. The efficiency of the device was calculated using standard methods established in the literature (14). The emission profile was also measured as a function of the angle to confirm that it has a Lambertian emission profile.

In our device structure, there is a significant imbalance in charge transport. The hole mobility of TAPC ($\sim 1.0 \times 10^{-2}$ cm^2 V^{-1} s^{-1}) (8) is 4 orders of magnitude higher than the electron mobility of BCP (5.5×10^{-6} cm^2 V^{-1} s^{-1}) (10). It is expected that the OLED device is strongly hole-dominant and the recombination zone is near the ETL (BCP) interface. Because the triplet energy of BCP is lower than that of FIrpic, triplet exciton quenching is expected at the BCP interface. To study the charge imbalance in this OLED structure, single-carrier devices corresponding to the OLED were also fabricated. The hole-only device has the following structure: ITO/PEDOT:PSS (25 nm)/HTL (200 nm)/EML (20 nm)/Au. The electron-only device has the following structure: ITO/EML (20 nm)/ETL (200 nm)/LiF (1 nm)/Al. In the hole-only device, Au has a large work function, and it is expected that it will not inject electrons. Similarly, ITO has a small work function, and it will not inject holes into the EML of the electron-only device.

Current−voltage measurements were performed on these devices. From the current density−voltage ($J-V$) data shown in Figure 2, it can be seen clearly that the hole current density is more than 4 orders of magnitude higher than the electron current density over a wide voltage range. Because of the charge imbalance in the device, it is expected that the recombination zone of the device is located at the EML/ETL interface. To verify the location of the recombination zone and the charge balance, three different OLEDs were fabricated. Device A is the control device with the entire host layer doped with FIrpic with the following structure: ITO/PEDOT/TAPC/mCP:FIrpic (20 nm)/BCP/LiF/Al. Device B (left-doped) has a partially FIrpic-doped host layer adjacent to the HTL with the following structure: ITO/PEDOT/TAPC/mCP:FIrpic (10 nm)/mCP (10 nm)/BCP/LiF/Al. Device C (right-doped) has a partially FIrpic-doped host layer adjacent to the ETL with the following structure: ITO/PEDOT/TAPC/mCP (10 nm)/mCP:FIrpic (10 nm)/BCP/LiF/Al. Because the device is electron-deficient, only a small fraction of electrons will be able to transport across the undoped host layer, and device B should have a lower efficiency. If the recombination is

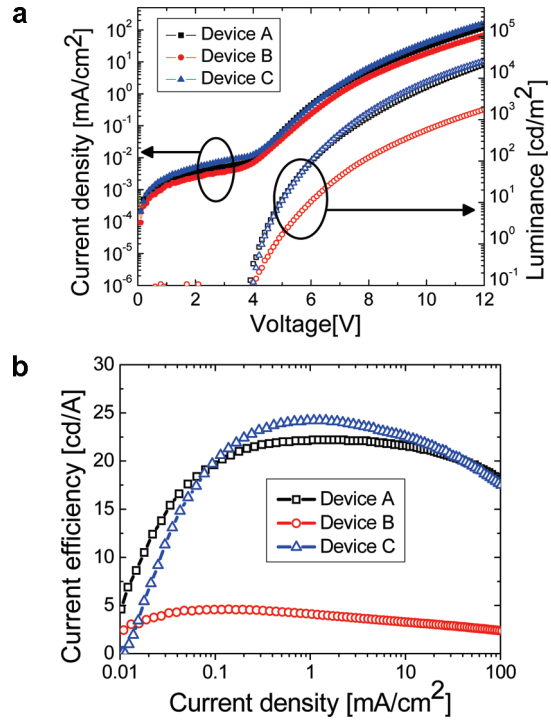

FIGURE 3. (a) LIV characteristics for devices A (control), B (left-doped) and C (right-doped). The filled symbols indicate the current density, whereas open symbols indicate luminance of the corresponding device. (b) Current efficiency for devices A (control), B (left-doped), and C (right-doped).

indeed located at the ETL interface, the efficiency of device C should be similar to that of the control device A. It should be noted that, in devices with mCP as a host, the charge carriers are transported through mCP and the presence of FIrpic does not affect the carrier transport in the EML (13), (15). Therefore, the exact location of the doped layer should not affect the carrier transport in the mCP layer. Figure 3a shows the LIV characteristics of these three devices. The current densities of the three devices are almost the same. These results are expected because FIrpic does not affect carrier transport in the host layer. It should be noted that the dual-carrier device current is, in general, higher than the single-carrier device current because of the space charge effect and carrier recombination. However, in our case, the hole-only device current in Figure 2 is almost the same as the dual-carrier device currents in Figure 3 because of the dominance of the hole current. In fact, the current in devices A and C is slightly higher than that in device B, indicating that devices A and C are more charge balanced. While the difference in the current is small, the difference in the current efficiency between these three devices is substantial. Device B has a substantially lower luminance compared to devices A and C, indicating that it has a lower efficiency. The efficiencies of these three devices are also shown in Figure 3b. The current efficiency of device B is less than 5 cd A^{-1}, which is substantially lower compared to the other two devices (>20 cd A^{-1}). The results indicate that in device B only a small portion of the electrons injected are able to transport across the undoped host layer and recombine with holes injected from the HTL, resulting in a low efficiency. On the basis of these data, it is apparent that in both devices

Table 1. Energy Level, Triplet Energy, and Mobility Parameters for Different ETMs Used in This Study

ETL	HOMO (eV)	LUMO (eV)	T_1 (eV)	mobility ($cm^2\ V^{-1}\ s^{-1}$)
BCP(10, 21)	6.5	3.0	2.5	10^{-6}
BPhen(18, 22)	6.4	3.2	2.5	10^{-4}
3TPYMB(16)	6.77	3.3	2.98	10^{-5}

A and C the recombination zone is located at the BCP interface. However, because BCP has a lower triplet energy than FIrpic, recombination at the BCP interface leads to triplet exciton quenching. If BCP is replaced with ETMs with higher electron mobility and higher triplet energy, the charge balance will be improved and exciton quenching will be reduced, resulting in a higher overall device efficiency.

In our present study, we chose tris[3-(3-pyridyl)mesityl]borane (3TPYMB) as an ETM because its electron mobility ($\sim 10^{-5}$ $cm^2\ V^{-1}\ s^{-1}$) (16) is about 1 order of magnitude higher than that of BCP and it has one of the highest triplet energies ($T_1 = 2.98$ eV) (17) among all ETMs used in OLEDs. To show the effect of electron transport due to 3TPYMB, electron-only devices using BCP and 3TPYMB along with 4,7-diphenyl-1,10-phenanthroline (BPhen) were fabricated. Here, BPhen ($T_1 = 2.5$ eV) (18) was also used because it has triplet energy similar to that of BCP, while its electron mobility (10^{-4} $cm^2\ V^{-1}\ s^{-1}$) is the highest among all three ETMs. The highest occupied molecular orbital (HOMO) and lowest unoccupied molecular orbital (LUMO) energy levels, triplet energies, and mobilities for all three ETMs have been summarized in Table 1. Figure 4a shows the $I-V$ characteristics

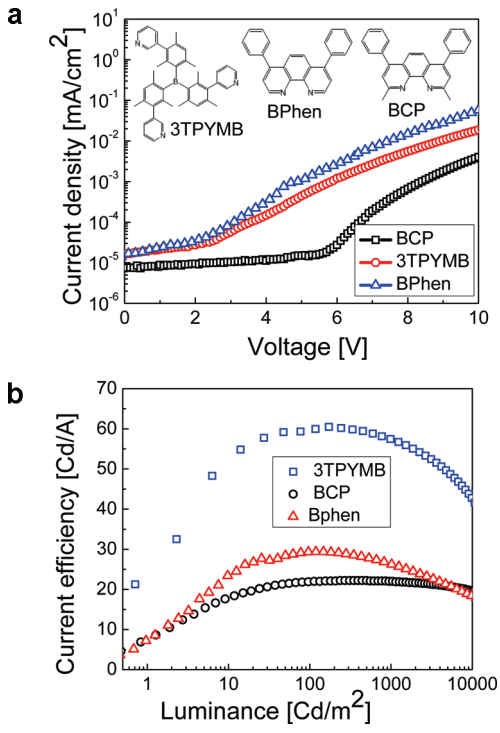

FIGURE 4. (a) $J-V$ characteristics of electron-only devices with BCP, 3TPYMB, and BPhen as the ETL showing the highest current density at a given voltage for BPhen, followed by 3TPYMB and the lowest for BCP. (b) Current efficiencies for OLED devices with BCP, 3TPYMB, and BPhen as the ETL.

of the three electron-only devices, and the results show that the BPhen device has the highest current density, followed by 3TPYMB and then the BCP devices. Those results are consistent with the mobility values of the corresponding ETMs.

To demonstrate the effect of the charge balance on the OLED device performance, we fabricated devices with three different ETMs. All of the devices show the characteristic emission of FIrpic, and no other emission is observed. Figure 4b shows the device efficiencies for all three devices. The BCP device has the lowest efficiency of all, which is in agreement with its lowest mobility and low triplet energy. Although the electron mobility of BPhen is substantially higher than those of the other two ETMs, because of its low triplet energy, the device efficiency is only slightly higher than that of the BCP device. Finally, the 3TPYMB device shows substantially higher efficiency (60 cd A^{-1}) compared to the other two devices. Similar efficiency has also been reported for FIrpic-based devices (19, 20). Our optimized 3TPYMB device shows a peak luminous power efficiency of 50 lm W^{-1}. The results demonstrate that both high-mobility and high-triplet-energy ETMs are required for high device efficiency.

In summary, the charge balance was studied in FIrpic-based blue-phosphorescent OLEDs, and the devices were found to be hole-dominant. We found that the recombination zone is located at the EML/ETL interface by selectively doping FIrpic in different regions of the host. Using 3TPYMB, the charge balance is enhanced. Because of the high electron mobility and high triplet energy in the ETL, a maximum current efficiency of 60 cd A^{-1} was demonstrated in FIrpic devices.

Acknowledgment. The authors acknowledge support by the Department of Energy Office of Energy Efficiency and Renewable Energy (Award DE-FC26-06NT42855).

REFERENCES AND NOTES

(1) Krummacher, B. C.; Choong, V.-E.; Mathai, M. K.; Choulis, S. A.; So, F.; Jermann, F.; Fiedler, T.; Zachau, M. *Appl. Phys. Lett.* **2006**, *88*, 113506.
(2) Forrest, S. R. *Nature* **2004**, *428*, 911–918.
(3) Baldo, M. A.; O'Brien, D. F.; You, Y.; Shoustikov, A.; Sibley, S.; Thompson, M. E.; Forrest, S. R. *Nature* **1998**, *395*, 151–154.
(4) Adachi, C.; Baldo, M. A.; Thompson, M. E.; Forrest, S. R. *J. Appl. Phys.* **2001**, *90*, 5048–5051.
(5) Lee, J.-H.; Lin, T.-C.; Liao, C.-C.; Yang, F. H. In *SPIE*; Gang, Y., Chuangtian, C., Changhee, L., Eds.; SPIE: Bellingham, WA, 2005; Vol. 5632, pp 220–225.
(6) Choong, V.-E.; Shi, S.; Curless, J.; Shieh, C.-L.; Lee, H. C.; So, F.; Shen, J.; Yang, J. *Appl. Phys. Lett.* **1999**, *75*, 172–174.
(7) So, F.; Krummacher, B.; Mathai, M. K.; Poplavskyy, D.; Choulis, S. A.; Choong, V.-E. *J. Appl. Phys.* **2007**, *102*, 091101.
(8) Strohriegl, P.; Grazulevicius, J. V. *Adv. Mater.* **2002**, *14*, 1439–1452.
(9) Lee, J.; Chopra, N.; Eom, S.-H.; Zheng, Y.; Xue, J.; So, F.; Shi, J. *Appl. Phys. Lett.* **2008**, *93*, 123306.
(10) Li, Y. Q.; Fung, M. K.; Xie, Z.; Lee, S. T.; Hung, L. S.; Shi, J. *Adv. Mater.* **2002**, *14*, 1317–1321.
(11) Goushi, K.; Kwong, R.; Brown, J. J.; Sasabe, H.; Adachi, C. *J. Appl. Phys.* **2004**, *95*, 7798–7802.
(12) Baldo, M. A.; Forrest, S. R. *Phys. Rev. B* **2000**, *62*, 10958.
(13) Holmes, R. J.; Forrest, S. R.; Tung, Y. J.; Kwong, R. C.; Brown, J. J.; Garon, S.; Thompson, M. E. *Appl. Phys. Lett.* **2003**, *82*, 2422–2424.

(14) Forrest, S. R.; Bradley, D. D. C.; Thompson, M. E. *Adv. Mater.* **2003**, *15*, 1043–1048.
(15) Chopra, N.; Lee, J.; Zheng, Y.; Eom, S.-H.; Xue, J.; So, F. *J. Appl. Phys.* **2008** Manuscript in preparation.
(16) Tanaka, D.; Takeda, T.; Chiba, T.; Watanabe, S.; Kido, J. *Chem. Lett.* **2007**, *36*, 262–263.
(17) Tanaka, D.; Agata, Y.; Takeda, T.; Watanabe, S.; Kido, J. *Jpn. J. Appl. Phys., Part 2* **2007**, *46*, L117—L119.
(18) Xin, Q.; Li, W. L.; Su, W. M.; Li, T. L.; Su, Z. S.; Chu, B.; Li, B. *J. Appl. Phys.* **2007**, *101*, 044512.
(19) Su, S.-J.; Sasabe, H.; Takeda, T.; Kido, J. *Chem. Mater.* **2008**, *20*, 1691–1693.
(20) Sasabe, H.; Gonmori, E.; Chiba, T.; Li, Y.-J.; Tanaka, D.; Su, S.-J.; Takeda, T.; Pu, Y.-J.; Nakayama, K.-I.; Kido, J. *Chem. Mater.* **2008**, *20*, 5951–5953.
(21) Ikai, M.; Tokito, S.; Sakamoto, Y.; Suzuki, T.; Taga, Y. *Appl. Phys. Lett.* **2001**, *79*, 156–158.
(22) Lei, G. T.; Wang, L. D.; Duan, L.; Wang, J. H.; Qiu, Y. *Synth. Met.* **2004**, *144*, 249–252.

AM900228B